## PAPER

Check for updates

# Valorisation of lignocellulose and low concentration $CO_2$ using a fractionation–photocatalysis–electrolysis process†

Santiago Rodríguez-Jiménez, [ID] ‡ Erwin Lam,‡ Subhajit Bhattacharjee [ID] and Erwin Reisner [ID] *

The simultaneous upcycling of all components in lignocellulosic biomass and the greenhouse gas $CO_2$ presents an attractive opportunity to synthesise sustainable and valuable chemicals. However, this approach is challenging to realise due to the difficulty of implementing a solution process to convert a robust and complex solid (lignocellulose) together with a barely soluble and stable gas ($CO_2$). Herein, we present the complete oxidative valorisation of lignocellulose coupled to the reduction of low concentration $CO_2$ through a three-stage fractionation–photocatalysis–electrolysis process. Lignocellulose from white birch wood was first pre-treated using an acidic solution to generate predominantly cellulosic- and lignin-based fractions. The solid cellulosic-based fraction was solubilised using cellulase (a cellulose depolymerising enzyme), followed by photocatalytic oxidation to formate with concomitant reduction of $CO_2$ to syngas (a gas mixture of CO and $H_2$) using a phosphonate-containing cobalt(II) bis(terpyridine) catalyst immobilised onto $TiO_2$ nanoparticles. Photocatalysis generated $27.9 \pm 2.0 \ \mu mol_{CO} \ g_{TiO_2}^{-1}$ ($TON_{CO}$ = 2.8 ± 0.2; 16% CO selectivity) and $147.7 \pm 12.0 \ \mu mol_{formate} \ g_{TiO_2}^{-1}$ after 24 h solar light irradiation under 20 vol% $CO_2$ in $N_2$. The soluble lignin-based fraction was oxidised in an electrolyser to the value-added chemicals vanillin ($0.62 \ g_{lignin}^{-1}$) and syringaldehyde ($1.65 \ g_{lignin}^{-1}$) at the anode, while diluted $CO_2$ (20 vol%) was converted to CO ($20.5 \pm 0.2 \ \mu mol_{CO} \ cm^{-2}$ in 4 h) at a Co(II) porphyrin catalyst modified cathode ($TON_{CO}$ = 707 ± 7; 78% CO selectivity) at an applied voltage of −3 V. We thus demonstrate the complete valorisation of solid and a gaseous waste stream in a liquid phase process by combining fractioning, photo- and electrocatalysis using molecular hybrid nanomaterials assembled from earth abundant elements.

## Introduction

The renewable generation of valuable chemicals and fuels is a critical step towards a sustainable chemical industry.[1,2] The valorisation of abundant waste resources, such as ligno-cellulosic biomass and the greenhouse gas $CO_2$ offers great potential to achieve such an ambitious goal at the scale required to defossilise our industry. By harnessing the power of renewable energy sources, such as solar and wind, the conversion of non-edible biomass and $CO_2$ *via* photo- or electrochemical approaches presents an opportunity to produce sustainable fuels and chemicals.[3]

Lignocellulosic biomass such as wood, is abundant and cheap and consists predominantly of three polymeric com-

ponents: cellulose, hemicellulose and lignin.[4,5] Cellulose and hemicellulose consist mainly of polysaccharide made from glucose, xylose, mannose and arabinose. Lignin is made of different polymerised aromatic units, and its utilisation remains challenging due to the robustness of its polyaromatic structure, which requires harsh conditions to break down the polymer (*e.g.*, strong acids such as $H_2SO_4$).[6,7] Unlike cellulose, lignin-to-chemical conversion technologies remain scarce.[4,5,7,8] An important linkage in lignin, often found between its aromatic polymeric backbone, is the β-O-4 bond between two phenyl rings, which serves as an ideal target to depolymerise lignin into smaller aromatic fragments.[9–11] The selective depoly-merisation of all lignocellulose components and their subsequent chemical transformation would enable large-scale access to aliphatic and aromatic renewable feedstock chemicals.

Apart from ubiquitous biomass sources, the greenhouse gas $CO_2$ can be used as an abundant carbon source to produce energy-rich chemicals such as CO, formate, hydrocarbons or alcohols.[12] However, photo- and electroreduction of $CO_2$ are predominantly performed in the presence of pure $CO_2$, where

concentrated $CO_2$ streams have to be generated involving additional energy input.[13–15] To alleviate the energy demand of the process, it is desirable to perform catalytic reactions at lower $CO_2$ concentrations (e.g., ≤20% $CO_2$).[16–20] The challenge of using low concentration $CO_2$ streams lies in maintaining high product selectivity and catalytic activity compared to reactions employing pure $CO_2$ streams.[17] Molecular $CO_2$ reduction catalysts display an increased product selectivity compared to most heterogeneous electro- or photocatalysts.[16,21,22]

An attractive approach to utilise biomass and $CO_2$ together is their simultaneous conversion in photo- or electrocatalytic processes.[23–25] This strategy opens the possibility to couple biomass oxidation with $CO_2$ reduction in a single process driven by sunlight or renewable electricity. The coupling of productive half-reactions thereby allows the conversion of a solid and a gaseous waste stream into valuable products such as CO, syngas, formate and aromatic chemicals, which can be more attractive than conventional systems performing overall water splitting to generate $H_2$ and $O_2$ from water. Additionally, the oxidation of biomass-derived substrates is thermodynamically less demanding than water oxidation, thereby facilitating the catalytic conversions, as well as the generation of value-added products.[26–28] This combined approach also allows for the isolation of products in different phases and compartments, which can help with product separation. Conventional approaches such as water splitting generate explosive $H_2$ and $O_2$ mixtures in the reactor headspace.

The valorisation of cellulose and $CO_2$ streams has recently been reported using a $TiO_2$ nanoparticle with an immobilised $CO_2$ reducing cobalt(II) bis(terpyridine) catalyst containing phosphonate anchors (**CotpyP**) ($TiO_2$|**CotpyP**). Photoexcitation of this hybrid $TiO_2$|**CotpyP** photocatalyst reduced aqueous $CO_2$ to syngas, while cellulose-derived glucose was simultaneously oxidised to formate and arabinose. $TiO_2$|**CotpyP** could operate for 24 h and be recycled up to three times.[29] However, only concentrated $CO_2$ and pure cellulose have been used, and no strategy for lignin separation and utilisation were reported in this previous study.

Herein, we report the valorisation of all components in lignocellulose coupled to low concentration $CO_2$ reduction, which has been achieved by employing molecular $CO_2$ reduction hybrid nanomaterials (Fig. 1). First, lignocellulose is pre-treated and fractioned into predominantly cellulosic- and lignin-based components using acid hydrolysis. Second, the fractionated cellulosic solution was converted with low concentration $CO_2$ using the $TiO_2$|**CotpyP** photocatalyst to $HCOO^-$ and syngas, respectively. Finally, an electrolysis process concomitantly converted the fractionated lignin solution on a carbon-based anode to vanillin and syringaldehyde, which find application in the food, pharma and cosmetics industries.[10,30] Diluted $CO_2$ is reduced to CO (with a single pass conversion yield close to 5% at both 10 vol% and 20 vol% $CO_2$) with a molecular cobalt(II) porphyrin (**CoP$_L$**) catalyst immobilised on a multiwall carbon nanotube (MWCNT) cathode. Thus, we demonstrate the complete valorisation of lignocellulose and low concentration $CO_2$, which has been

enabled by a precious-metal free fractionation–photocatalysis–electrolysis process.

# Results and discussion

### Fractionation of lignocellulose

The composition of dried and extracted white birch wood used in this study was determined by quantifying its sugar and lignin composition following standard characterisation procedures using $H_2SO_4$ hydrolysis:[6] glucose (34.7 ± 1.6 wt%), xylose (20.3 ± 1.0 wt%), mannose (1.8 ± 0.1 wt%), arabinose (0.9 ± 0.1 wt%) and lignin (17.6 ± 1.4 wt%). Further details are provided in the Experimental section, Fig. 1, Fig. S1 and Tables S1 and S2.†

To effectively utilise the different components of lignocellulose, their individual components are first separated by acid hydrolysis. Lignocellulose was pre-treated in a dioxane/HCl/HCOOH mixture at 80 °C for 3 h (500 mg in 5.9 mL) to obtain a liquid (or liquor) and a solid fraction.[7] The dioxane/HCl/HCOOH mixture solubilises lignin and the liquid fraction predominantly consisted of lignin (41.2 ± 2.1 wt%) along with xylose (6.9 ± 1.3 wt%), glucose (2.4 ± 0.6 wt%), mannose (1.3 ± 0.3 wt%) and arabinose (2.5 ± 0.7 wt%). The second most abundant component xylose (derived from hemicellulose) is partially converted to furfural under these fractioning conditions (see Experimental section, and Fig. 1, Fig. S1 and Tables S1–S3† for further details).[26] The isolated solid fraction consisted mainly of cellulosic components such as glucose (62.9 ± 1.9 wt%) and xylose (6.7 ± 1.6 wt%) with some lignin (5.4 ± 1.2 wt%).

### Photocatalytic valorisation of cellulose and $CO_2$

The solid fraction obtained from lignocellulose fractionation contained mainly cellulose and was used as a feedstock in photocatalysis following depolymerisation via cellulase pre-treatment.[29] The depolymerised glucose and cellobiose are suitable electron donors in semiconductor suspension systems,[31] and their valorisation has been previously reported.[32,33] Specifically, the solid fraction was enzyme pre-treated with cellulase (0.05 $mg_{cellulase}$ $mg_{solid}^{-1}$) to generate soluble sugars, predominantly glucose (39.3 ± 4.7 mM) and cellobiose (8.7 ± 2.1 mM) after 24 h incubation at 37 °C in an aqueous sodium acetate buffer solution (50 mM) at pH 5.[29] With respect to white birch, 10.2 ± 0.4 wt% and 4.2 ± 0.6 wt% were converted to glucose and cellobiose, respectively (see Tables S1 and S2†).

The lignocellulose-derived sugar solution was then utilised for $CO_2$ reduction reactions using the $TiO_2$|**CotpyP** photocatalyst (Fig. 1).[29] In a typical experiment, **CotpyP** (50 nmol) was added to a photoreactor containing a $TiO_2$ suspension (5 mg, P25, particle diameter ~20 nm) in 2 : 1 MeCN : cellulase-treated solid fraction aqueous solution (3 mL). The photoreactor was sealed with a rubber septum and purged with 100% $CO_2$ or 20% $CO_2$ (balanced with $N_2$) at a flow rate of 15 mL $min^{-1}$ for 15 min. The sealed and stirred photoreactor was irradiated with a solar light simulator
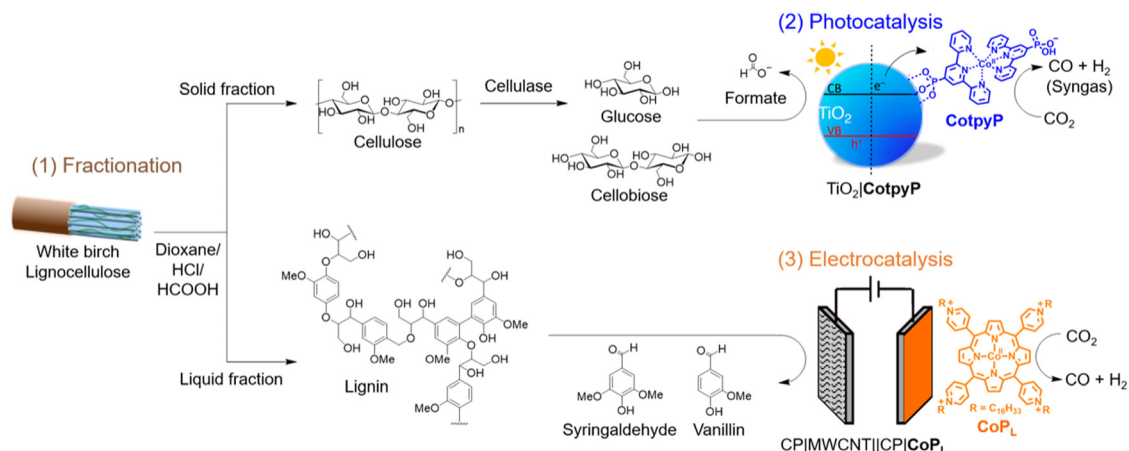
**Fig. 1** Schematic overview of a three-stage process for the complete valorisation of lignocellulose and diluted $CO_2$. (1) Fractionation of lignocellulose from white birch into a predominant cellulose and lignin fraction (top and bottom, respectively), with the cellulose-based solid fraction being further incubated in cellulase to generate a soluble sugar (glucose and cellobiose) solution. Structures of xylose, mannose and arabinose are omitted for clarity. (2) Photocatalytic oxidation of cellulose-derived glucose and cellobiose to formate coupled with reduction of diluted $CO_2$ to syngas (CO and $H_2$) using $TiO_2$|**CotpyP** photocatalyst. (3) Electrolytic oxidation of lignin to aromatic aldehydes syringaldehyde and vanillin coupled with reduction of diluted $CO_2$ to CO and $H_2$ using CP|MWCNT||CP|**CoP$_L$**.

(100 mW cm$^{-2}$, AM 1.5G, 25 °C, 600 rpm) for 24 h. The UV in the full solar spectrum is necessary to photoexcite electrons from the valence to the conduction band of $TiO_2$.[29] The gaseous products ($H_2$ and CO) in the headspace (4.74 mL) were quantified by gas chromatography (GC), and $HCOO^-$ formed in the solution from glucose photooxidation was quantified by ion chromatography.

After 24 h of photocatalysis under 100 vol% $CO_2$, 69.9 ± 4.0 μmol$_{CO}$ g$_{TiO_2}^{-1}$, 109.8 ± 8.0 μmol$_{H_2}$ g$_{TiO_2}^{-1}$ (*i.e.*, 39% CO and 61% $H_2$ selectivity for gaseous products) and 153.7 ± 4.0 μmol$_{formate}$ g$_{TiO_2}^{-1}$ were formed. Under 20 vol% $CO_2$, the formation yields were 27.9 ± 2.0 μmol$_{CO}$ g$_{TiO_2}^{-1}$, 141.7 ± 27.9 μmol$_{H_2}$ g$_{TiO_2}^{-1}$ (*i.e.*, 16% CO and 84% $H_2$ selectivities) and 147.7 ± 12.0 μmol$_{formate}$ g$_{TiO_2}^{-1}$ (Fig. 2a and Table S4†). The obtained CO yields correspond to a $CO_2$-to-CO conversion yield of ~0.03% and ~0.05% at 100 vol% and 20 vol% $CO_2$, respectively. The reduction of protons (from water) to $H_2$ and $CO_2$ to CO by **CotpyP** as well as the oxidation of glucose/cellobiose by $TiO_2$ to formate are two-electron processes with an expected 1:1 stoichiometric ratio for ($H_2$ + CO):formate, which is close to the observed ratios.[29,34–36]

The carbon source of the products was confirmed by isotopic labelling experiments. Experiments with $^{13}CO_2$ and cellulase enzyme pre-treated cellulose were performed to confirm that the CO originates from $CO_2$ reduction (for further details see Experimental section). Analysis of the gas headspace after photocatalysis by transmission IR spectroscopy reveals that $^{13}CO$ produced by $TiO_2$|**CotpyP** was only formed when $^{13}CO_2$ was used as the carbon source (Fig. 2b). Furthermore, in the case of formate, based on previous work using $^{13}C_6$-glucose with $TiO_2$|**CotpyP**, $^{13}C$-formate is only formed through the photooxidation of $^{13}C_6$-glucose, confirming formate's carbon source.[29] Further mechanistic insights of the photooxidation of glucose to formate can be found in ref. 36.

These results demonstrate that the cellulose solid fraction, following cellulase pre-treatment, provides a source of suitable electron donors for photocatalytic $CO_2$ reduction. The solar $TiO_2$|**CotpyP** reforming system was able to convert $CO_2$-to-CO at concentrations of 20 vol% $CO_2$, with an activity drop of only a factor of two despite the five-fold drop in $CO_2$ concentration with respect to 100 vol% $CO_2$ (Fig. 2a). Near stoichiometric amounts of $HCOO^-$ to CO/$H_2$ were formed at both $CO_2$ concentrations, demonstrating the effectiveness of $TiO_2$|**CotpyP** to photooxidise sugars to formate and concomitantly photoreduce $CO_2$ and $H_2O$ to CO and $H_2$.

### Electrolytic valorisation of lignin and $CO_2$

To optimise the simultaneous electrolysis of $CO_2$ and lignin, the half-reactions of electroreduction of low $CO_2$ concentration and electrooxidation of lignocellulose-derived lignin were first studied individually in a three-electrode setup. This was followed by the proof-of-concept coupling of both half reactions in a two-electrode electrolyser using the optimised cathode and anode.

Low concentration $CO_2$ electroreduction was performed on **CoP$_L$** immobilised on MWCNT as a molecular catalyst (see Fig. 1). **CoP$_L$** was chosen based on its known CO selectivity during electroreduction of pure $CO_2$, and stability when immobilised on MWCNT *via* π–π stacking and its lipophilic alkyl chains (see ESI Note 1, and Fig. S2–S4†).[28,37] We therefore further explored the electroreduction ability of **CoP$_L$** supported on MWCNT under variable $CO_2$ concentrations ranging 10, 20, 50 and 100 vol% (balanced with $N_2$), using an electrochemical flow setup that allowed continuous purging of the electrolyte solution with a given gas composition.[38]

Cathodes containing **CoP$_L$** were prepared, following a reported procedure (see Fig. S5†),[28] by drop-casting a dimethylformamide (DMF) suspension containing 2.37 mg

**Fig. 2** (a) $H_2$, CO and formate (blue, green and red, respectively) formation after 24 h of photocatalysis with TiO₂|**CotpyP**. (b) Transmission IR spectra with $^{13}CO_2$ isotopic labelling of the headspace after 24 h of photocatalysis (sample, green curve), including $^{12}CO$ (black) and $^{13}CO$ (red) as reference. Reaction conditions: 5 mg TiO₂ (P25); 50 nmol **CotpyP**; 3 mL 2 : 1 MeCN : pre-treated reaction solution (cellulose fraction pre-treated with cellulase); 25 °C, 100 mW cm⁻², AM 1.5G. (a) 20 vol% $CO_2$ was balanced with $N_2$; (b) sample (green) was purged with 100% $^{13}CO_2$. Experiments in (a) were performed in triplicates.



**Fig. 3** (a) Chronoamperometry (CA) experiments as a function of concentration of $CO_2$ and time during $CO_2$ electrochemical reduction to CO using CP|**CoP$_L$** cathodes. (b) CO formation rate and selectivity during CA experiments. Experiments were performed in triplicates, and the shaded area represents the standard deviation. Reaction conditions: CA: 0.1 M NaHCO₃ in H₂O (pH = 6.7); $E_{app}$ = −1.2 V vs. Ag/AgCl for 3.5 h; WE: CP|**CoP$_L$**, CE: Pt foil, RE: Ag/AgCl (sat. KCl). Flow of $CO_2$ : $N_2$ 9 mL min⁻¹. $CO_2$ concentration was varied stepwise between 0 vol%, 10 vol%, 20 vol%, 50 vol% and 100 vol% and balanced with $N_2$.

MWCNT mL⁻¹ and 0.1 mM **CoP$_L$** onto carbon paper (CP) (0.1 mL$_{DMF}$ cm⁻², geometrical surface area = 1 cm²), which is denoted as CP|**CoP$_L$**. Electrocatalysis with CP|**CoP$_L$** was performed in a two-compartment electrochemical cell with a three-electrode setup. Pt foil was used as the counter electrode (CE) and Ag/AgCl (sat. KCl) as reference electrode (RE), a Nafion membrane separating the cathode and anode chambers, with the catholyte (0.1 M NaHCO₃ in H₂O) under a constant gas flow (9 mL min⁻¹) of $CO_2$ and $N_2$ regulated by mass flow controllers. The generated gaseous products during electrochemical experiments ($H_2$ and CO) were measured via online GC (schematically represented in Fig. S6†).[38]

During chronoamperometry (CA) experiments, under an applied potential of −1.2 V vs. Ag/AgCl (sat. KCl) the catholyte chamber was continuously purged with pure $N_2$ for 30 min, after which the $CO_2$ concentration was gradually increased to 10, 20, 50 and 100 vol% every 45 min (Fig. 3a). Under pure $N_2$, the current density was the lowest at approximately −0.5 mA cm⁻² and around ~0.08 μmol$_{H_2}$ min⁻¹ evolved as the main gaseous product, with a minor CO background (<0.01 μmol$_{CO}$ min⁻¹) likely caused by the chemical equilibrium between carbonic acid ($H_2CO_3$) and $CO_2$. Upon increasing the $CO_2$ concentration (in vol%), the current density gradually increased, from approximately −0.8 mA cm⁻² (10 vol%), to −1.2 mA cm⁻²

(20 vol%), to −1.5 mA cm⁻² (50 vol%) and to −1.8 mA cm⁻² (100 vol%). The $H_2$ formation rate remained constant at ~0.06 μmol$_{H_2}$ min⁻¹ at all $CO_2$ concentration steps, whereas the CO formation rate and CO selectivity increased from ~0.12 μmol$_{CO}$ min⁻¹ and ~65% (10 vol%), to ~0.24 μmol$_{CO}$ min⁻¹ and ~80% (20 vol%), to ~0.35 μmol$_{CO}$ min⁻¹ and ~90% (50 vol%) and to ~0.50 μmol$_{CO}$ min⁻¹ and ~93% (100 vol%) (Fig. 3b). The low $H_2$ formation rate across all studied $CO_2$ concentrations (~0.06 μmol$_{H_2}$ min⁻¹) may be explained by the high affinity of **CoP$_L$** to $CO_2$.[28] The carbon source of CO was previously confirmed for **CoP$_L$** through $^{13}CO_2$ isotopic labelling experiments.[28,37]

Two main observations can be made by screening different $CO_2$ gas flow concentrations: (1) **CoP$_L$** exhibits a high product specificity with around ~80% CO selectivity even under 20 vol% of substrate $CO_2$. (2) The CO formation rate at 20 vol% $CO_2$ (~0.24 μmol$_{CO}$ min⁻¹; CO turnover frequency (TOF$_{CO}$) = 8.3 min⁻¹; single-pass $CO_2$ conversion yield[39] = 4.7%) corresponds to roughly half the activity with respect to 100 vol% $CO_2$ (~0.50 μmol$_{CO}$ min⁻¹; TOF$_{CO}$ = 17.2 min⁻¹; single-pass $CO_2$

conversion yield = 2.0%), thus indicating that decreasing five-fold the $CO_2$ concentration only reduces two-fold the CO formation rate (Fig. 3b).

When comparing CP|$CoP_L$ with $TiO_2$|$CotpyP$, both molecular hybrid systems exhibit similar CO formation rate trends, although CP|$CoP_L$ maintains higher CO selectivity across all $CO_2$ concentrations (see ESI Note 1 and Tables S4 and S5†). The origin of the observed trends for $TiO_2$|$CotpyP$ and CP|$CoP_L$ at different $CO_2$ concentrations remains unclear but may be attributed to their molecular structure, which provides intrinsic affinity towards $CO_2$. In comparison with state-of-the-art molecular systems, such as the rhenium bipyridine electrocatalyst [Re(4,4-dimethyl-2,2-dipyridyl)(CO)$_3$(triethanolamine)], which operates in a DMF/triethanolamine solvent mixture at variable $CO_2$ concentrations (1, 10 and 100%) under comparable flow conditions,[22] CP|$CoP_L$ is three orders of magnitude more active (i.e., $TOF_{CO}$ = 0.5 h$^{-1}$ after 24 h at 10% $CO_2$ vs. 413 h$^{-1}$ after 4 h at 20% $CO_2$, respectively). Without taking into account that $CO_2$ is more soluble in organic solvents than in water (e.g. ~180 mM in DMF vs. ~33 mM in water at 25 °C), these differences in performance could be tentatively associated to the catalytic mechanism of $CO_2$ reduction, which enables cobalt porphyrins to achieve higher TOF than rhenium bipyridine electrocatalysts.[22,37]

The electrooxidation of the liquid fraction or liquor, containing predominantly lignin and obtained from pre-treating lignocellulose (250 mg), was studied in a two-compartment electrochemical cell with a three-electrode setup. For this purpose, the anodic conditions were initially optimised using the lignin model substrate 1-(3,4-dimethoxyphenyl)-2-(2-methoxyphenoxy)propane-1,3-diol, which contains a β-O-4 linkage between two phenyl rings that mimics those ubiquitously found in lignin (see Fig. 1 and Fig. S7†).[9–11]

CP|MWCNT anodes were fabricated by dropcasting a MWCNT suspension in ethanol (1.67 mg mL$^{-1}$, 0.1 mL cm$^{-2}$) containing Nafion 117 (2 vol% of a 5 wt% solution) to achieve a high surface area MWCNT layer with ~20 μm thickness (see Fig. S8†). We found that MWCNT on hydrophilic carbon paper (CP|MWCNT) acted as a suitable catalyst for the oxidation of the β-O-4 linkage in the model substrate (see Fig. S7 and ESI Note 2†). CP|MWCNT (geometric surfaced area = 1 cm$^2$) in the presence of 10 mM of lignin model substrate in 0.1 M $Na_2CO_3$ in 1 : 1 MeCN : $H_2O$ achieved high current densities (~8 mA cm$^{-2}$) at +1 V vs. Ag/AgCl (sat. KCl), while in absence of lignin, and under the same conditions, the current densities were lower (~3 mA cm$^{-2}$) (see Fig. S9 and S10†). MeCN was used to increase the solubility of the lignin model substrate and lignin. The generated oxidation product from the lignin model substrate during CA experiments, 3,4-dimethoxybenzaldehyde (3,4-MBA), was obtained in 36 ± 1% yield with a faradaic yield (FY) of 25 ± 1% assuming a two-electron oxidation (see Experimental details, Fig. S11 and Table S6†). The obtained 3,4-dimethoxybenzaldehyde was measured by $^1$H nuclear magnetic resonance (NMR) spectroscopy in CDCl$_3$ with mesitylene as internal standard (see Fig. S12–S14†).

Having established the optimised conditions (see ESI Note 3, and Fig. S15–S20†) and the electrodes suitable for lignin oxidation and low concentration $CO_2$ reduction, we aimed at coupling both redox half reactions in a single two-electrode electrolyser with the corresponding anolytes and catholytes separated by a bipolar membrane. Electrolysis was performed using a two-electrode setup (CP|$CoP_L$ as WE and CP|MWCNT as CE) with an applied voltage ($U_{app}$) of −3 V for 4 h. The anolyte comprised of 0.1 M $Na_2CO_3$ in a 1 : 1 MeCN : $H_2O$ solvent mix containing lignin (obtained from pre-treating 250 mg lignocellulose), and the catholyte had 0.1 M $NaHCO_3$ in $H_2O$. The catholyte was constantly purged at 9 mL min$^{-1}$ with 20 vol% $CO_2$ (balanced with $N_2$). The gaseous products on the cathodic side were monitored by online GC.[38]

During 4 h electrolysis, the initial current density gradually decreased from approximately −1.4 mA cm$^{-2}$ to around −0.4 mA cm$^{-2}$ (Fig. S21†), and the initial maximum CO formation rate observed changed from ~0.2 μmol$_{CO}$ min$^{-1}$ to ~0.05 μmol$_{CO}$ min$^{-1}$ (Fig. 4a and b). After 4 h, 20.5 ± 0.2 μmol$_{CO}$ cm$^{-2}$ was produced along with 5.8 ± 0.3 μmol$_{H_2}$ cm$^{-2}$ ($TON_{CO}$ = 707 ± 7 and $TON_{H_2}$ = 200 ± 10) corresponding to a CO selectivity of 78 ± 2% and a $FY_{CO+H_2}$ of 59 ± 6% (Table S5†). Despite of the decrease in current density and CO formation rates, the CO selectivity remained stable.[28]

After electrolysis, the anolyte was worked-up (see Experimental section for details) and the crude product was analysed by $^1$H NMR spectroscopy in CDCl$_3$. Control experiments, where the lignin fraction was stirred in the electrolyte solution for 4 h without applied bias, led to the formation of a small background level of aldehydes. Importantly, under an applied potential more aromatic aldehyde signals were formed (Fig. S20† and Fig. 4c), which shows that aromatic monomer formation is promoted by electrooxidation. The observed $^1$H NMR signals corresponded to syringaldehyde and vanillin (see Fig. 1 and 4c), which are aromatics that can be formed from lignin.[8,10] After 4 h CA, 0.14 ± 0.03 μmol and 0.31 ± 0.03 μmol of vanillin and syringaldehyde were detected, respectively. These yields equated to 0.62 g of vanillin and 1.65 g of syringaldehyde per kilogram of lignin. Compared with oxygen evolved from water oxidation, vanillin and syringaldehyde have potential as bio-derived monomers in the polymer industry.[40] The observed moderate yields for vanillin and syringaldehyde could be attributed to the acidic degradation of reaction intermediates, i.e., lignin-fragment oxidation decreased the local pH at the CP|MWCNT anode surface below 11.5, and hence halt the formation of the targeted aromatics.[40] In addition to the two identified aromatic compounds, other unidentified signals in the aromatic aldehyde (~9.8 ppm) and methoxy regions (3.8–4.0 ppm) can be observed in the $^1$H NMR spectra (Fig. 4c).[40]

In comparison to CP|MWCNT, the use of heterogeneous anodes for lignin oxidation based on metals/metal oxides, such as toxic Pb/PbO$_2$, has been previously reported.[41–43] For instance, these Pb/PbO$_2$ anodes were able to generate different lignin-derived products, such as vanillin (5.83 g kg$_{lignin}^{-1}$) and syringaldehyde (9.30 g kg$_{lignin}^{-1}$), via electrooxidation/electro-

**Fig. 4** Electrolysis of 20 vol% $CO_2$ gas flow with CP|$CoP_L$ at the cathode coupled to lignin conversion at the anode with CP|MWCNT. (a) Current density as a function of time. (b) CO formation rate and selectivity during electrolysis at the cathode. (c) $^1H$ NMR spectrum recorded in $CDCl_3$ of the anolyte containing lignin after 4 h electrocatalysis showing the emergence of aldehydes and methoxy groups. Experiments were performed in triplicates, and the standard deviation are represented as shaded area (a, b). Reaction conditions: (a and b) Electrolysis (two electrode configuration) at $U_{app} = -3$ V. Anolyte: 0.1 M $Na_2CO_3$, lignin fraction obtained from pre-treating 250 mg lignocellulose in 1 : 1 MeCN : $H_2O$; anode: CP|MWCNT. Catholyte: 0.1 M $NaHCO_3$ in $H_2O$ with a flow of 20 vol% $CO_2$ (balanced with $N_2$) 9 mL $min^{-1}$; cathode: CP|$CoP_L$; bipolar membrane; room temperature. (c) The asterisk (*) highlights the additional aldehyde signal formed from lignin electrooxidation.

hydrogenation of bamboo-derived lignin when used with Cu cathodes in 1 M NaOH solution.[41] Despite the difficulty to compare this previously reported system with our CP|MWCNT||CP|$CoP_L$ system due to the different experimental conditions (*i.e.*, electrode materials and surface, pH, tempera-ture, substrate concentration, applied voltage and currents), the metal-free CP|MWCNT anodes were able to generate yields of vanillin and syringaldehyde within the same order or one-order of magnitude lower than those reported for the metal/metal oxide based Pb/$PbO_2$||Cu system.

Previous work has shown that lignin valorisation can be coupled with hydrogen evolution or reduction of $CO_2$ to formate using photoelectrochemical systems.[44,45] In comparison, our work presents a unique and successful three-stage approach that shows that complete valorisation of ligno-cellulose is possible through the combination of fractionation and utilisation of photocatalysis and electrocatalysis to oxidise the resulting solid fraction to formate and liquid fraction to aromatics and reduce diluted $CO_2$ and water to CO and $H_2$. Although this system is a proof-of-concept demonstration, different factors would need consideration for practical implementation. These include optimisation of catalyst per-formance, scalability,[46,47] integration of a carbon capture step,[48] potential limitations such as catalyst stability, the engineering design of reactors[49,50] for lignocellulose fraction-ation,[46] photocatalysis[51] and electrolysis,[52] and the separation of products for further use.[53,54]

## Conclusions

We report a combined fractionation-photocatalysis-electroly-sis process for the complete valorisation of lignocellulose and low-concentration $CO_2$. Fractioning lignocellulosic wood provides sugar-based solid and lignin-based soluble fractions that are photo- and electrocatalytically converted with immobilised molecular cobalt(II) catalysts to produce CO, formate, vanillin and syringaldehyde. The presented results set a precedent in integrating renewable processes for com-plete waste feedstock valorisation under ambient pressure and temperature. Moreover, our molecular hybrid systems were able to convert low $CO_2$ concentrations (10–20 vol% $CO_2$), which paves the way towards utilising $CO_2$ concen-trations nearing those found in flue gas (4–10 vol% $CO_2$). However, to utilise actual flue gas additional $CO_2$ purifi-cation steps are necessary to eliminate impurities,[55] such as $SO_2$, $SO_3$, $NO_x$, $O_2$ and particulate matter depending on the type of fuel used. Learning from the use of low $CO_2$ concen-tration also brings us a step closer towards operating directly from atmospheric $CO_2$ (420 ppm).[20,56]

Hence, this work demonstrates a proof-of-concept strategy to valorise challenging multicomponent waste streams simul-taneously through solar-driven and electrochemical redox pro-cesses. This work further highlights the potential of molecu-larly engineered hybrid materials[57] in the valorisation of waste streams, which can be expanded beyond $CO_2$ reduction in future developments to perform chemistry in a more sustain-able and circular manner. As biomass and $CO_2$ emerge as the most scalable and readily available sustainable carbon sources to defossilise the chemical industry,[58] this work aims to inspire new approaches in their practical valorisation.

# Experimental section

## Solvents and materials

Acetonitrile (MeCN, Fisher Chemicals), $D_2O$ (Sigma Aldrich), D(+)-glucose (Fisher Chemicals), D(+)-cellobiose (Acros), Cellulase from *Trichoderma reesei* ATCC 26921 (Sigma Aldrich), sodium acetate trihydrate (Fisher Chemicals), hydrochloric acid (34–37% Fisher Chemicals), 1-(3,4-dimethoxyphenyl)-2-(2-methoxyphenoxy)propane-1,3-diol (lignin model substrate, FluoroChem), Vanillin (Thermo Scientific), syringaldehyde (Thermo Scientific), vanillic acid (Sigma Aldrich), syringic acid (Thermo Scientific), fufural (Sigma Aldrich), 2-methoxyphenoxyacetic acid (Alfa Aesar), 3,4-dimethoxybenzaldehyde (Acros), 4-hydroxybenzoic acid (Thermo Scientific), white birch (Merck), dioxane (Fisher Chemicals), formic acid (Fisher Chemicals), sulfuric acid (Fisher Chemicals), multiwalled carbon nanotubes (MWCNT 755117, Sigma Aldrich), carbon paper (Toray Paper 60, Fuel Cell Store), Nafion solution (5 wt% Sigma Aldrich), $NaHCO_3$ (Merck), EtOAc (Fisher Chemicals), THF (Fisher Chemicals), $Na_2CO_3$ (Merck), $MgSO_4$ (Fisher Chemicals) $CDCl_3$ (Sigma Aldrich), 50 wt% $H_2SO_4$ (Fluka), $Na_2CO_3$ 64 mM and $NaHCO_3$ 20 mM (ion chromatography eluent concentrate for Metrosep A Supp5; Sigma Aldrich) were purchased from commercial sources and used as received. MilliQ® grade $H_2O$ was used for all the experiments. $TiO_2$ powder P25 (10–30 nm diameter; 50 $m^2$ $g^{-1}$) was obtained from Evonik; $[Co(2,2':6',2''-terpyridine-4'-phosphonic\ acid)_2]$ $(BF_4)_2$ (denoted as **CotpyP**)[35] and **CoP$_L$**[37] were synthesised according to reported procedures. Reaction gases ($CO_2$ and $N_2$) were purchased from BOC. Ag/AgCl reference electrode was stored in a saturated NaCl solution (sat. NaCl; BasiMW-2030) and anion exchange membrane (Selemion, AGC Engineering), Nafion 117 membrane (Sigma Aldrich), bipolar membrane (Fumacep, Fuel Cell Store), were stored in MilliQ® grade $H_2O$.

## Physical characterisation

$^1H$ NMR spectroscopy was recorded on a Bruker DPX 400 MHz spectrometer with the chemical shifts ($\delta$) of the $^1H$ NMR spectrum being referenced against the residual solvent signal ($D_2O$: $\delta$ = 4.79 ppm, $CDCl_3$: $\delta$ = 7.26 ppm). Scanning electron microscopy was performed on a TESCAN MIRA3 FEG-SEM instrument. Before measuring the samples, they were sputtered with 10 nm of platinum.

## Product quantification

Gaseous $H_2$ and CO under static conditions were analysed by a Shimadzu Tracera GC-2010 Plus with a barrier discharge ionization detector. The GC-2010 Plus was equipped with a ShinCarbon micro ST column (0.53 mm diameter) kept at 40 °C using helium carrier gas. The response factors for the gases were determined by calibration with known amounts of $H_2$ and CO. Typically, 50 μL of headspace gas from the photoreactor was injected using an air-tight syringe (Hamilton, GASTIGHT). Formate was analysed by ion chromatography (IC) on a Metrohm 882 compact IC plus chromatography system equipped with a Metrosep A Supp 5 – 150/4.0 column using an aqueous $Na_2CO_3$ (3.2 mM) and $NaHCO_3$ (1 mM) solution as eluent. The response factor of formate was determined by calibration with known amounts of aqueous formate solutions. Sugar concentrations (glucose, cellobiose, xylose, mannose and arabinose) were determined by high performance liquid chromatography (HPLC) on a Waters Breeze system equipped with a refractive index detector and a Rezex 8% $Ca^{2+}$ Monosaccharide 300 × 7.80 mm HPLC column using 2.5 mM $H_2SO_4$ as the eluent with a flow rate of 0.5 mL $min^{-1}$ (at 75 °C). The response factors for the sugars were determined by calibration of aqueous sugar solutions with known amounts of sugar.

## Klason lignin and sugar content determination

Klason lignin and sugar determination was performed following a reported procedure.[6] For the compositional analysis of white birch, the sample was first dried at 105 °C overnight followed by cooling to room temperature under static vacuum in a desiccator containing $CuSO_4$ as drying agent. The dried solid was extracted three times with an ethanol : water mixture (4 : 1 v/v and 20 mL $g^{-1}$) followed by water (20 mL $g^{-1}$) by sonication for 30 min. The sample was then dried at 105 °C overnight followed by cooling to room temperature under static vacuum in a desiccator containing $CuSO_4$ as a drying agent.

To determine the Klason lignin content and sugar concentration, to 250 mg of the solid (dried and extracted white birch or solid after white birch pre-treatment in dioxane/HCl/HCOOH) was added 3.75 mL of a 72 wt% $H_2SO_4$ at room temperature. The suspension was stirred periodically (every 15 min with a glass rod) for 2 h and 145 mL of MilliQ® grade $H_2O$ was added, followed by refluxing the suspension at 120 °C for 4 h. The suspension was filtered on a tared frit. The solid was dried at 105 °C overnight and the mass of the filtered solid was determined gravimetrically to determine Klason Lignin content. The filtrate was diluted with $H_2O$ to 250 mL and concentrated to 50 mL at 80 °C. The solution was then analysed by HPLC to determine the sugar content (glucose, xylose, mannose, galactose and arabinose).

To determine the Klason Lignin and sugar content of the liquor from white Birch pre-treatment in dioxane/HCl/HCOOH, the liquor obtained from pre-treating 500 mg white Birch was used following the same procedure as with dried and extracted white Birch.

## White Birch pre-treatment

Lignocellulose fractioning was performed following a reported procedure.[7] To 500 mg of dried and extracted white birch was added dioxane (4.5 mL), conc. HCl (0.42 mL), formic acid (0.36 mL) and water (0.64 mL). The suspension was then stirred for 5 h at 80 °C and filtered and the residue was washed with dioxane until the solution became clear (solid/cellulose fraction). The combined filtrate was dried at 60 °C under vacuum and extracted with THF followed by drying at 40 °C to obtain a dark oil (liquid/lignin fraction).

**Enzyme hydrolysis of pre-treated white Birch**

The obtained solid after treatment of white birch with dioxane/HCl/HCOOH was washed three times with $H_2O$ (20 mL $g^{-1}$) to remove residual HCOOH and dried at 105 °C overnight. To the washed and dried solid fraction (150 mg) in an aqueous sodium acetate solution (50 mM, 3 mL) at pH 5 (adjusted by the addition of HCl) at 37 °C was added cellulase (15 mg in 0.75 mL) in a 50 mM aqueous sodium acetate solution at pH 5. The suspension was incubated at 37 °C for 24 h, followed by 15 min at 90 °C and filtration through a syringe filter (0.2 μm). The filtered solution was stored at −4 °C. The pre-treated cellulose fraction solution contained glucose (39.3 ± 4.7 mM) and cellobiose (8.7 ± 2.2 mM) as determined by HPLC. Control experiments with the recovered solid after treatment of white Birch with dioxane/HCl/HCOOH under the same condition in the absence of cellulase did not show the formation of glucose or cellobiose.

**CP|MWCNT electrode preparation**

A suspension containing MWCNT in ethanol (1.67 mg $mL^{-1}$) and 2 vol% of a 5 wt% Nafion solution was sonicated for 15 minutes. The suspension was then dropcasted on a defined area of carbon paper (0.1 mL $cm^{-2}$) that was masked with Teflon tape followed by overnight drying at room temperature. The electrode was then taped to a metal rod using a copper tape and the metal rod and copper tape were wrapped with Parafilm.

**CP|CoP$_L$ electrode preparation**

A suspension containing MWCNT in DMF (3.16 mg $mL^{-1}$) was sonicated for 10 min. Subsequently, this ink was diluted 25% by adding 0.4 mM **CoP$_L$** in DMF to achieve 2.37 mg MWCNT $mL^{-1}$ and 0.1 mM **CoP$_L$**. This ink was further sonicated for 10 min and then dropcasted on a defined area (masked with Teflon tape) of carbon paper (0.1 mL $cm^{-2}$), followed by drying overnight at room temperature. The electrode was then taped to a metal rod using a copper tape and the metal rod and copper tape were wrapped with Parafilm.

**Photocatalytic experiments**

In a typical experiment, to $TiO_2$ (P25, 5 mg) was added 2 mL of MeCN and 1 mL of the solution obtained from cellulase pre-treatment in a glass photoreactor (7.74 mL total volume) equipped with a magnetic stir bar. 50 nmol of **CotpyP** (from a freshly prepared 2 mM solution in $H_2O$; 0.025 mL) was added, and the photoreactor (3 mL solution with 4.74 mL headspace) was capped with a rubber septum and purged with $CO_2$ (100 vol% or 20 vol% balanced with $N_2$) controlled by mass flow controllers for 15 min at 15 mL $min^{-1}$, followed by stirring for 15 min in the dark. The photoreactor (kept at 25 °C and stirred at 600 rpm) was then irradiated with a calibrated solar light simulator (Newport Oriel, 100 mW $cm^{-2}$) equipped with an air mass 1.5 global (AM 1.5G) filter and a water filter to remove infrared radiation. The photocatalytic process was monitored by analysing the headspace after 6 and 24 h by gas chromatography to monitor $H_2$ and CO formation. Formate in the solu-

tion (diluted in $H_2O$ (1:9 v:v photocatalysis solution:$H_2O$)) was analysed at the end of the photocatalytic studies (after 24 h) by ion chromatography.

**$CO_2$-to-CO conversion yield**

Photocatalytic $CO_2$-to-CO conversion yield (%) of $TiO_2$|**CotpyP** was calculated by dividing the mol of CO produced after 24 h by the mol of $CO_2$ in the photoreactor headspace and multiplying the product by 100. The mol of $CO_2$ was obtained using the ideal gas law equation ($pV = nRT$), where $p$ is 1 atm, $V$ is the volume of the reactor headspace in L multiplied by the molar fraction of $CO_2$, $R$ is the ideal gas constant (0.082 atm L $mol^{-1}$ $K^{-1}$) and $T$ is 298.15 K.

**Isotopic labelling experiments**

To a suspension of cellulose (300 mg) in a 50 mM aqueous sodium acetate solution (6 mL) at pH 5 (adjusted by the addition of HCl) at 37 °C was added cellulase (15 mg in 1.5 mL) in a 50 mM aqueous sodium acetate solution at pH 5. The suspension was incubated at 37 °C for 24 h, followed by 15 min at 90 °C and filtration through a syringe filter (0.2 μm). The filtered solution was stored at −4 °C. The pre-treated cellulose solution contained glucose (53 ± 2 mM) and cellobiose (26 ± 1 mM) as determined by HPLC. To a glass photoreactor vial (7.74 mL total volume) equipped with a magnetic stir bar was added 5 mg of $TiO_2$ which was suspended in 2.95 mL of 2:1 v:v MeCN:pre-treated cellulose solution. The molecular catalyst **CotpyP** (0.025 mL 50 nmol, 2 mM in $H_2O$) and 0.025 mL $H_2O$ (to reach 3 mL) was added and the photoreactor was capped with a rubber septum. The photoreactor was then degassed for one min (vacuum at $10^{-2}$ mbar) after which $^{13}CO_2$ (1 bar) was introduced. The photoreactor (kept at 25 °C and stirred at 600 rpm) was then irradiated (AM 1.5G, 100 mW $cm^{-2}$). The headspace was then transferred to an air-tight evacuated IR cell (10 cm path length, equipped with KBr windows) and the background (IR cell under vacuum) corrected IR spectrum was recorded to detect $^{12}CO$ and $^{13}CO$.

**Flow $CO_2$ electroreduction**

Electrochemical experiments were performed on an Ivium Compactstat electrochemical analyser controlled by the Iviumsoft software. In a typical three-electrode setup experiment, a 0.1 M $NaHCO_3$ solution in $H_2O$ was prepared and used as the anolyte and catholyte separated by a Nafion membrane. CA was performed with CP|**CoP$_L$** as working electrode, Pt foil as counter electrode and Ag/AgCl as reference electrode. The electrochemical cell was capped with rubber septa and the catholyte was purged for 30 minutes with $N_2$ (for screening electrocatalytic performance of different gas composition) or the desired gas composition (for CA at a given gas composition (20 or 100 vol%) for 4 h) at a flow rate of 20 mL $min^{-1}$ controlled by mass flow controllers (Brooks) to remove oxygen. Afterwards the flow rate was reduced to 9 mL $min^{-1}$ and a potential of −1.2 V $vs.$ Ag/AgCl was applied. CA was run at −1.2 V $vs.$ Ag/AgCl for 4 h at constant gas flow of 20 or 100 vol% or during screening different gas composition, the electro-

catalytic activity was measured for 30 min under $N_2$ followed by increasing the $CO_2$ concentration to 10, 20, 50 and 100 vol% every 45 min. Electrochemical experiments were carried out at room temperature. The formed gaseous products ($H_2$ and CO) were measured by online GC measurement (injection every 4.5 min) using an Shimadzu Tracera GC-2010 Plus gas chromatograph equipped a barrier discharge ionization detector.[38] Calibration was performed by determining the response factor by flowing a calibration gas with known CO and $H_2$ composition under the same condition (9 mL min$^{-1}$).

### Electrocatalytic lignin model substrate & lignin oxidation

Electrochemical experiments were performed in three-electrode configuration on a PalmSens MultiEMStat$^{3+}$ potentiostat. In a typical experiment, 0.1 M $Na_2CO_3$ solution in MeCN : $H_2O$ (1 : 1 vol%) was used as the electrolyte. To the electrolyte was added 0.01 M of the lignin model substrate or the lignin fraction from pre-treating 250 mg white birch in dioxane/HCl/$H_2O$. The solution was then used as anolyte (8 mL) in electrocatalysis with 0.1 M $Na_2CO_3$ solution in MeCN : $H_2O$ (1 : 1 vol%), and separated from the catholyte by a Selemion anion exchange membrane, and the electrochemical cell was capped with rubber septa. Cyclic voltammetry (CV) or CA were performed with CP|MWCNT as working electrode, Pt foil as counter electrode and Ag/AgCl (sat. KCl) as reference electrode. CV scans were run from −0.2 to 1.0 V vs. Ag/AgCl followed by a backwards scan to −0.2 V vs. Ag/AgCl with a scan rate of 50 mV s$^{-1}$. CA experiments were performed for 4 h at 1.0 V vs. Ag/AgCl. Electrochemical experiments were carried out at room temperature. To analyse the products after electrocatalysis, the anolyte was acidified to a pH of 3 with 0.1 M HCl, extracted with EtOAc (3 × 5 mL), dried over $MgSO_4$, filtered and dried at 40 °C under vacuum to obtain a light brown solid. The solid was further analysed by $^1H$ NMR spectroscopy in $CDCl_3$ with mesitylene as internal standard. Control experiments were performed without an applied potential and stirring the anolyte containing the lignin model substrate or lignin fraction for 4 h followed work up and analysis by $^1H$ NMR spectroscopy in $CDCl_3$.

### Electrocatalytic lignin oxidation coupled to $CO_2$ reduction

Electrochemical experiments were performed in two-electrode configuration on an Ivium Compactstat electrochemical analyser controlled by the Iviumsoft software. In a typical experiment a 0.1 M $Na_2CO_3$ solution in MeCN : $H_2O$ (1 : 1 vol%) was prepared and used for the electrolyte. To the electrolyte was added 0.01 M of the lignin model substrate or the lignin fraction from pre-treating 250 mg white birch in dioxane/HCl/$H_2O$. The solution was then used as anolyte (4 mL). A 0.1 M $NaHCO_3$ solution in $H_2O$ was used as catholyte. The anolyte and catholyte were separated by a bipolar membrane. Electrolysis was performed with CP|MWCNT and CP|**CoP**$_L$ as anode and cathode, respectively. The electrochemical H-type cell was capped with two rubber septa and the catholyte was purged for 30 minutes with 20 vol% $CO_2$ (balanced by $N_2$) at a flow rate of 20 mL min$^{-1}$ controlled by mass flow controllers (Brooks) to remove oxygen. Afterwards the flow rate was reduced to 9 mL min$^{-1}$ and a potential of $U_{app}$ = −3 V was applied and run for 4 h. Electrochemical experiments were carried out at room temperature. The formed gaseous products ($H_2$ and CO) on the cathode side were measured by online GC measurement (injection every 4.25 min) using Shimadzu Tracera GC-2010 Plus gas chromatograph equipped a barrier discharge ionization detector.[38] Calibration was performed by determining the response factor by flowing a calibration gas with known CO and $H_2$ composition under the same condition (9 mL min$^{-1}$). To analyse the products, after electrocatalysis the anolyte was acidified to a pH of 3 with 0.1 M HCl, extracted with EtOAc (3 × 5 mL), dried over $MgSO_4$, filtered and dried at 40 °C under vacuum to obtain a light brown solid. The solid was further analysed by $^1H$ NMR in $CDCl_3$ with mesitylene as internal standard. Control experiments were performed under the same conditions but without the lignin model substrate or lignin fraction dissolved in the anolyte.

### Single-pass $CO_2$ conversion yield

The electrochemical single-pass $CO_2$ conversion yield (%) of CP|**CoP**$_L$ was calculated by dividing the rate of CO formation (mol min$^{-1}$) by the flow rate of $CO_2$ (mol min$^{-1}$) and multiplying the product by 100. The flow rate of $CO_2$ was obtained by transforming mL min$^{-1}$ to mol min$^{-1}$ using the ideal gas law equation ($pV = nRT$), where $p$ is 1 atm, $V$ is the flow rate of $CO_2$ in L min$^{-1}$ (e.g., $1.8 \times 10^{-3}$ L min$^{-1}$ for 20 vol% $CO_2$), $R$ is the ideal gas constant (0.082 atm L mol$^{-1}$ K$^{-1}$) and $T$ is 298.15 K.

### Data analysis

Experiments were performed in triplicates and the results are represented with the mean ($\bar{x}$) and standard deviation ($\sigma_{\bar{x}}$) expressed as $\bar{x} \pm \sigma_{\bar{x}}$ with

$$\bar{x} = \frac{1}{n} \sum_{i=1}^{n} x_i$$

$$\sigma_{\bar{x}} = \sqrt{\frac{1}{(n-1)} \sum_{i=1}^{n} (x_i - \bar{x})^2}$$

where $n$ is the number of measurements and $x_i$ the individually determined value.

## Conflicts of interest

There are no conflicts to declare.

## Acknowledgements

# References

1 S. C. Peter, *ACS Energy Lett.*, 2018, **3**, 1557–1561.

2 G. W. Huber, S. Iborra and A. Corma, *Chem. Rev.*, 2006, **106**, 4044–4098.

3 R. Schlögl, *Green Chem.*, 2021, **23**, 1584–1593.

4 W. Schutyser, T. Renders, S. Van den Bosch, S. F. Koelewijn, G. T. Beckham and B. F. Sels, *Chem. Soc. Rev.*, 2018, **47**, 852–908.

5 X. Liu, X. Duan, W. Wei, S. Wang and B.-J. Ni, *Green Chem.*, 2019, **21**, 4266–4289.

6 TAPPI T 222 om-02, 2006 (Technical Association of the Pulp and Paper Industry, **https://www.tappi.org/content/ sarg/t222.pdf**).

7 L. Shuai, M. T. Amiri, Y. M. Questell-Santiago, F. Héroguel, Y. Li, H. Kim, R. Meilan, C. Chapple, J. Ralph and J. S. Luterbacher, *Science*, 2016, **354**, 329–333.

8 M. M. Abu-Omar, K. Barta, G. T. Beckham, J. S. Luterbacher, J. Ralph, R. Rinaldi, Y. Román-Leshkov, J. S. M. Samec, B. F. Sels and F. Wang, *Energy Environ. Sci.*, 2021, **14**, 262–292.

9 C. Zhang and F. Wang, *Acc. Chem. Res.*, 2020, **53**, 470–484.

10 Z. Sun, B. Fridrich, A. de Santi, S. Elangovan and K. Barta, *Chem. Rev.*, 2018, **118**, 614–678.

11 M. Rafiee, M. Alherech, S. D. Karlen and S. S. Stahl, *J. Am. Chem. Soc.*, 2019, **141**, 15266–15276.

12 A. M. Appel, J. E. Bercaw, A. B. Bocarsly, H. Dobbek, D. L. DuBois, M. Dupuis, J. G. Ferry, E. Fujita, R. Hille, P. J. A. Kenis, C. A. Kerfeld, R. H. Morris, C. H. F. Peden, A. R. Portis, S. W. Ragsdale, T. B. Rauchfuss, J. N. H. Reek, L. C. Seefeldt, R. K. Thauer and G. L. Waldrop, *Chem. Rev.*, 2013, **113**, 6621–6658.

13 A. C. Forse and P. J. Milner, *Chem. Sci.*, 2021, **12**, 508–516.

14 S. E. Renfrew, D. E. Starr and P. Strasser, *ACS Catal.*, 2020, **10**, 13058–13074.

15 E. Pérez-Gallent, C. Vankani, C. Sánchez-Martínez, A. Anastasopol and E. Goetheer, *Ind. Eng. Chem. Res.*, 2021, **60**, 4269–4278.

16 T. Nakajima, Y. Tamaki, K. Ueno, E. Kato, T. Nishikawa, K. Ohkubo, Y. Yamazaki, T. Morimoto and O. Ishitani, *J. Am. Chem. Soc.*, 2016, **138**, 13818–13821.

17 G. Lee, Y. C. Li, J.-Y. Kim, T. Peng, D.-H. Nam, A. Sedighian Rasouli, F. Li, M. Luo, A. H. Ip, Y.-C. Joo and E. H. Sargent, *Nat. Energy*, 2021, **6**, 46–53.

18 A. Khurram, M. He and B. M. Gallant, *Joule*, 2018, **2**, 2649–2666.

19 A. Khurram, L. Yan, Y. Yin, L. Zhao and B. M. Gallant, *J. Phys. Chem. C*, 2019, **123**, 18222–18231.

20 S. Kar, M. Rahaman, V. Andrei, S. Bhattacharjee, S. Roy and E. Reisner, *Joule*, 2023, **7**, 1496–1514.

21 A. Perazio, G. Lowe, R. Gobetto, J. Bonin and M. Robert, *Coord. Chem. Rev.*, 2021, **443**, 214018.

22 H. Kumagai, T. Nishikawa, H. Koizumi, T. Yatsu, G. Sahara, Y. Yamazaki, Y. Tamaki and O. Ishitani, *Chem. Sci.*, 2019, **10**, 1597–1606.

23 X. Du, H. Zhang, K. P. Sullivan, P. Gogoi and Y. Deng, *ChemSusChem*, 2020, **13**, 4318–4343.

24 C. Yang, S. Maldonado and C. R. J. Stephenson, *ACS Catal.*, 2021, **11**, 10104–10114.

25 D. T. Whipple and P. J. A. Kenis, *J. Phys. Chem. Lett.*, 2010, **1**, 3451–3458.

26 M. F. Kuehnel and E. Reisner, *Angew. Chem., Int. Ed.*, 2018, **57**, 3290–3296.

27 A. V. Puga, *Coord. Chem. Rev.*, 2016, **315**, 1–66.

28 S. Bhattacharjee, M. Rahaman, V. Andrei, M. Miller, S. Rodríguez-Jiménez, E. Lam, C. Pornrungroj and E. Reisner, *Nat. Synth.*, 2023, **2**, 182–192.

29 E. Lam and E. Reisner, *Angew. Chem., Int. Ed.*, 2021, **60**, 23306–23312.

30 A. K. Sinha, U. K. Sharma and N. Sharma, *Int. J. Food Sci. Nutr.*, 2008, **59**, 299–326.

31 T. Kawai and T. Sakata, *Nature*, 1980, **286**, 474–476.

32 J. C. Colmenares, A. Magdziarz and A. Bielejewska, *Bioresour. Technol.*, 2011, **102**, 11254–11257.

33 L. Da Vià, C. Recchi, E. O. Gonzalez-Yañez, T. E. Davies and J. A. Lopez-Sanchez, *Appl. Catal., B*, 2017, **202**, 281–288.

34 N. Elgrishi, M. B. Chambers and M. Fontecave, *Chem. Sci.*, 2015, **6**, 2522–2531.

35 J. J. Leung, J. Warnan, K. H. Ly, N. Heidary, D. H. Nam, M. F. Kuehnel and E. Reisner, *Nat. Catal.*, 2019, **2**, 354–365.

36 L. Lan, H. Daly, R. Sung, F. Tuna, N. Skillen, P. K. J. Robertson, C. Hardacre and X. Fan, *ACS Catal.*, 2023, **13**, 8574–8587.

37 S. Rodríguez-Jiménez, H. Song, E. Lam, D. Wright, A. Pannwitz, S. A. Bonke, J. J. Baumberg, S. Bonnet, L. Hammarström and E. Reisner, *J. Am. Chem. Soc.*, 2022, **144**, 9399–9412.

38 C. D. Sahm, G. M. Ucoski, S. Roy and E. Reisner, *ACS Catal.*, 2021, **11**, 11266–11277.

39 C. P. O'Brien, R. K. Miao, S. Liu, Y. Xu, G. Lee, A. Robb, J. E. Huang, K. Xie, K. Bertens, C. M. Gabardo, J. P. Edwards, C.-T. Dinh, E. H. Sargent and D. Sinton, *ACS Energy Lett.*, 2021, **6**, 2952–2959.

40 M. Fache, B. Boutevin and S. Caillol, *ACS Sustainable Chem. Eng.*, 2016, **4**, 35–46.

41 M. Liu, Y. Wen, J. Qi, S. Zhang and G. Li, *ChemistrySelect*, 2017, **2**, 4956–4962.

42 P. Parpot, A. P. Bettencourt, A. M. Carvalho and E. M. Belgsir, *J. Appl. Electrochem.*, 2000, **30**, 727–731.

43 C. Lan, H. Fan, Y. Shang, D. Shen and G. Li, *Sustainable Energy Fuels*, 2020, **4**, 1828–1836.

44 J. King and S. S. C. Chuang, *Catal. Commun.*, 2021, **149**, 106219.

45 D. Wang, S. H. Lee, S. Han, J. Kim, N. V. T. Trang, K. Kim, E.-G. Choi, P. Boonmongkolras, Y. W. Lee, B. Shin, Y. H. Kim and C. B. Park, *Green Chem.*, 2020, **22**, 5151–5160.

46 D. M. Alonso, S. H. Hakim, S. Zhou, W. Won, O. Hosseinaei, J. Tao, V. Garcia-Negron, A. H. Motagamwala, M. A. Mellmer, K. Huang, C. J. Houtman, N. Labbé, D. P. Harper, C. T. Maravelias, T. Runge and J. A. Dumesic, *Sci. Adv.*, 2017, **3**, e1603301.

47 E. Cooreman, T. Vangeel, K. Van Aelst, J. Van Aelst, J. Lauwaert, J. W. Thybaut, S. Van den Bosch and B. F. Sels, *Ind. Eng. Chem. Res.*, 2020, **59**, 17035–17045.

48 H. Ababneh, A. AlNouss and S. A. Al-Muhtaseb, *Processes*, 2022, **10**, 2406.

49 C. Song, W. Pan, S. T. Srimat, J. Zheng, Y. Li, Y.-H. Wang, B.-Q. Xu and Q.-M. Zhu, in *Studies in Surface Science and Catalysis*, ed. S.-E. Park, J.-S. Chang and K.-W. Lee, Elsevier, 2004, vol. 153, pp. 315–322.

50 H. A. Ruiz, M. Conrad, S.-N. Sun, A. Sanchez, G. J. M. Rocha, A. Romaní, E. Castro, A. Torres, R. M. Rodríguez-Jasso, L. P. Andrade, I. Smirnova, R.-C. Sun and A. S. Meyer, *Bioresour. Technol.*, 2020, **299**, 122685.

51 H. Nishiyama, T. Yamada, M. Nakabayashi, Y. Maehara, M. Yamaguchi, Y. Kuromiya, Y. Nagatsuma, H. Tokudome, S. Akiyama, T. Watanabe, R. Narushima, S. Okunaka, N. Shibata, T. Takata, T. Hisatomi and K. Domen, *Nature*, 2021, **598**, 304–307.

52 A. Caravaca, W. E. Garcia-Lorefice, S. Gil, A. de Lucas-Consuegra and P. Vernoux, *Electrochem. Commun.*, 2019, **100**, 43–47.

53 X. Ma, J. Albertsma, D. Gabriels, R. Horst, S. Polat, C. Snoeks, F. Kapteijn, H. B. Eral, D. A. Vermaas, B. Mei, S. de Beer and M. A. van der Veen, *Chem. Soc. Rev.*, 2023, **52**, 3741–3777.

54 M. Peer, S. Mehdi Kamali, M. Mahdeyarfar and T. Mohammadi, *Chem. Eng. Technol.*, 2007, **30**, 1418–1425.

55 P. Wattanaphan, T. Sema, R. Idem, Z. Liang and P. Tontiwachwuthikul, *Int. J. Greenhouse Gas Control*, 2013, **19**, 340–349.

56 S. J. Cobb, A. M. Dharani, A. R. Oliveira, I. A. C. Pereira and E. Reisner, *Angew. Chem. Int. Ed.*, 2023, **62**, e202218782.

57 K. E. Dalle, J. Warnan, J. J. Leung, R. Bertrand, I. S. Karmel and E. Reisner, *Chem. Rev.*, 2019, **119**, 2752–2875.

58 DECHEMA, FutureCamp, Roadmap Chemie 2050, *Verband der Chemischen Industrie e.V.*, **https://www.vci.de/vci/downloads-vci/publikation/2019-10-09-studie-roadmap-chemie-2050-treibhausgasneutralitaet.pdf**, 2023.